$2p_F$ and $4p_F$ instabilities in a one-quarter-filled-band Hubbard model

J. E. Hirsch
Institute for Theoretical Physics, University of California, Santa Barbara, California 93106 and Department of Physics, University of California, San Diego, California 92093

D. J. Scalapino
Department of Physics and Institute for Theoretical Physics, University of California, Santa Barbara, California 93106

(Received 18 February 1983)

The zero-frequency wave-vector-dependent charge- and spin-density susceptibilities for a quarter-filled-band extended Hubbard model are calculated with the use of a Monte Carlo technique. Results for a variety of different temperatures are given. Coulomb interactions are found to suppress the $2p_F$ charge-density response and enhance the $2p_F$ spin-density response. While a strictly on-site Coulomb interaction gives rise to only a weak $4p_F$ structure in the charge-density response, longer-range Coulomb interactions such as the near-neighbor interaction V in the extended Hubbard model can produce a singularity at $4p_F$. In addition to these susceptibilities, both the charge and spin structure factors are calculated, as well as two-particle, two-hole correlation functions. We also show some results for the ground-state energy, magnetic susceptibility, and specific heat of the Hubbard model. The relationship of the results obtained from our Monte Carlo simulations to various limiting exact results as well as to the well-known weak coupling renormalization-group predictions are discussed.

I. INTRODUCTION

Quasi-one-dimensional organic charge-transfer compounds have been the subject of intensive experimental and theoretical research in recent years.[1-3] Basic to an understanding of such materials is a detailed knowledge of the properties of one-dimensional interacting electron and electron-phonon systems. In this paper we begin a systematic study of the extended Hubbard[4] model using a recently developed Monte Carlo (MC) procedure.[5,6] This approach, proceeding via numerical simulation, is intermediate between theoretical and experimental studies, allowing one to obtain insight into the way thermodynamic properties and correlation functions depend on the parameters of a model. It has already proved to be effective for the study of certain one-dimensional models with electron-electron and electron-phonon interactions.[5-7]

Numerical simulations provide a complement to theoretical calculations. For example, they allow us to move away from weak or strong coupling solutions as well as various exact solutions to intermediate regimes which are often closest to experiment. They allow us to calculate a variety of thermodynamic properties as well as examine both short-range and long-range correlations. Simulations can indicate the range of validity of perturbation expansions. Fitted to renormalization-group scaling relations, they can carry out the first few renormalization steps giving the appropriate initial conditions to describe a specific model. Beyond this, the approach we have developed generates typical configurations of the system[6] which can give insight into the physics. In addition, simulations give results for "measurements" on well-defined model systems, which can be directly compared with experimental results on real materials. In this way one may learn whether a given model contains the essential physics of a problem. If so, by varying, for example, the size of the couplings or the band filling, one can systematically explore the relationship between the microscopic model and the resulting macroscopic physics. If the results do not agree with experiment, one knows to look further for the basic physics rather than argue that the failure is a result of an approximate solution. Conversely, simulations can also help one avoid the problem of using an approximate solution to obtain a rough fit to the data when in fact an accurate solution would fail to fit showing that the model does not contain the basic physics.

This paper contains results of a study of a one-quarter-filled-band extended Hubbard model with an on-site Coulomb interaction U and a near-

neighbor Coulomb interaction V. As is well known, both the charge- and spin-density zero-frequency susceptibilities of a noninteracting one-dimensional electron gas have a low-temperature $\ln T$ divergence at a momentum transfer of $2p_F$. This behavior of the charge-density susceptibility can give rise to a giant Kohn anomaly resulting in a peak in the diffuse x-ray scattering at $2p_F$ and, below a critical temperature, to a Peierls transition.[8]

Following the initial observations of $2p_F$ charge-density waves in the partially oxidized tetracyanoplatinate complex (Krogmann's salt) (KCP) and tetrathiafulvalene-tetracyanoquinodimethane (TTF-TCNQ), structures at $2p_F$ and sometimes also at $4p_F$ have been found in many quasi-one-dimensional systems.[9] Torrance[10] suggested that the structure at $4p_F$ was associated with strong long-range Coulomb interactions giving rise to the formation of a Wigner-type crystal.

An alternative explanation of the $4p_F$ anomaly involving moderate to strong Coulomb interactions was proposed by Emery.[11] In Emery's picture, the electron-phonon coupling of the lattice to the electronic charge density gives, in the usual way, the $2p_F$ Kohn anomaly and Peierls transition. He then associates the $4p_F$ anomaly with an instability arising from a correlated state of the $2p_F$ charge-density waves. Specifically, Emery argued that for intermediate to strong Coulomb interactions the two-particle two-hole susceptibility diverges at low temperatures at a wave vector $4p_F$. Then coupling this to the lattice via an electron-phonon interaction leads to a Kohn-Peierls behavior at $4p_F$ in a similar manner as the single-particle single-hole susceptibility gives rise to the $2p_F$ behavior.

We have calculated the momentum-dependent zero-frequency charge- and spin-density susceptibilities, and the effect of Coulomb interactions on the structure of these susceptibilities at momentum transfers $2p_F$ and $4p_F$. The two-particle, two-hole susceptibilities associated with on-site $n_{i\uparrow}n_{i\downarrow}$ and near-neighbor $n_{i+1}n_i$ Coulomb couplings were also evaluated along with the charge and spin structure factors. In Sec. II these susceptibilities and structure factors are defined and the form of the extended Hubbard model is given. The Monte Carlo procedure is introduced and some results for the Hubbard model (the near-neighbor coupling V of the extended Hubbard model is set to zero) are compared with exact results in the weak and strong U coupling limits. The calculated ground-state energy and magnetic susceptibility for various values of U are compared with Shiba's[12] exact results, and the temperature dependence of the specific heat and spin susceptibility for an intermediate value of U are given.

In Sec. III results for the Hubbard-model charge- and spin-correlation functions are given along with results for the two-particle, two-hole response. The temperature dependence of the charge and spin zero-frequency susceptibilities are shown for various values of the Coulomb interaction U and the charge and spin structure factors are plotted. The effect of the Coulomb interaction U is to suppress the $2p_F$ peak in the charge-density susceptibility and to enhance it in the spin-density response. Only a weak nonsingular structure is found for finite U in the charge-density response at $4p_F$. The $4p_F$ response is enhanced by longer-range Coulomb interactions, and in Sec. V we turn to the extended Hubbard model. No significant structure is observed in the two-particle, two-hole susceptibilities generated by the on-site or near-neighbor operators in the Hubbard model. This is in agreement with calculations in the $U=0$ and $U=\infty$ limits, and we believe that this type of four-particle process is suppressed by phase space and is not responsible for the $4p_F$ structure.

In Sec. IV we compare the Monte Carlo data with the weak coupling renormalization-group (RG) predictions.[3] This is of interest both as a check on the Monte Carlo calculation and to gain insight into the RG results. In the usual phase diagram constructed from the RG calculations, the zero-frequency $2p_F$ charge-density-wave (CDW) and spin-density-wave (SDW) susceptibilities both diverge as $(\epsilon_c/kT)^\alpha$ with $\alpha=N(0)U/2$ to leading order in $N(0)U$. However, as discussed in Sec. III, the Monte Carlo data show that the $2p_F$ peak in the charge-density response is suppressed while that in the spin-density response is enhanced as U is increased. The resolution of this puzzle is discussed in Sec. IV, where we find on integrating the nonlinear RG equations that indeed the $2p_F$ peak in the charge-density response is first suppressed by U and only at unphysically low temperatures is the fixed-point behavior $(\epsilon_c/kT)^\alpha$ achieved.

In Sec. V results obtained for the extended Hubbard model are given. Here, with both U and V present, structure is observed in the charge-density susceptibility at $4p_F$, and the structure at $2p_F$ is strongly suppressed. We thus find that for a one-quarter-filled band ($\rho=0.5$), Coulomb interaction can produce a $4p_F$ peak in the charge-density susceptibility but that when this happens the $2p_F$ peak is suppressed. In Sec. VI we summarize our findings.

II. THE MODEL AND SOME LIMITING RESULTS

In quasi-one-dimensional organic materials the molecules form stacks along which the intermolecular electronic orbital overlap is much greater than the overlap between molecules from different stacks.

The relative separation of the stacks also has the consequence that the electron-electron Coulomb interactions and the electron-ion interactions along a stack are stronger than those between stacks. Here we focus on the properties of a single chain leaving the question of how to treat the interchain coupling open. One approach which has been used to treat arrays of weakly coupled chains is to determine the properties of a single chain and to then treat the weak coupling between chains by a mean-field description.[13]

Consider a one-dimensional tight-binding electron system of bandwidth $4t$, with t the nearest-neighbor hopping matrix element. We will assume that the dominant Coulomb interactions are given by the on-site repulsion of electrons of opposite spin on the same molecule U. We will also consider the effect of adding a nearest-neighbor repulsion between electrons on neighboring molecules V. There is no difficulty in studying longer-range interactions with our Monte Carlo technique, but in this paper we restrict our attention to U and V, which are presumably the dominant interactions in most cases. The model of interest is then defined by

$$H=-t\sum_{i,\sigma}(C^{\dagger}_{i\sigma}C_{i+1,\sigma}+\text{H.c.})+U\sum_i n_{i\uparrow}n_{i\downarrow} +V\sum_i n_i n_{i+1}\,, \tag{2.1}$$

with $\sigma=\uparrow,\downarrow$ and $n_i=n_{i\uparrow}+n_{i\downarrow}$. Here, as noted in the Introduction, we consider only the one-quarter-filled-band sector.

For $V=0$, the Hubbard model defined by (2.1) can be studied exactly by Bethe-Ansatz techniques, as shown by Lieb and Wu.[14] However, this solution provides only limited information about the system: The ground-state energy, the energy gap, the zero-temperature magnetic susceptibility,[12] and the nearest-neighbor correlation function have been obtained exactly. It appears very difficult to obtain exact results for long-range correlation functions and for thermodynamic properties. For more than on-site interactions ($V\neq 0$), the model does not seem to be solvable by Bethe-Ansatz techniques.

The strictly one-dimensional system defined by Eq. (2.1) will, of course, not have a phase transition at any finite temperature but rather is characterized by the behavior of various low-temperature zero-frequency susceptibilities. For example, for a noninteracting system the charge-density susceptibility

$$N(q)=\int_0^{\beta}d\tau\langle\rho_q(\tau)\rho_q^{\dagger}(0)\rangle\,, \tag{2.2}$$

with $\rho_q^{\dagger}=\sum_{ps}C^{\dagger}_{p+q,s}C_{ps}$, exhibits the well-known $\ln(\epsilon_c/kT)$ low-temperature divergence at $q=2p_F$. Here ϵ_c is a cutoff energy related to the bandwidth. For an interacting system, calculations based upon the fixed-point limit of the weak coupling RG predict power-law divergences $(\epsilon_c/kT)^{\alpha}$ for the low-temperature susceptibilities. The actual phase transition of a quasi-one-dimensional system depends on both the size of the single-chain susceptibility and the strength of the appropriate interchain coupling.

Here we will study the single-chain zero-frequency charge-density and spin-density susceptibilities

$$N(q)=\frac{1}{N}\int_0^{\beta}d\tau\sum_{i,l}\langle[n_{i\uparrow}(\tau)+n_{i\downarrow}(\tau)] \times[n_{i+l\uparrow}(0)+n_{i+l\downarrow}(0)]\rangle e^{iql} \tag{2.3}$$

and

$$\chi(q)=\frac{1}{N}\int d\tau\sum_{i,l}\langle[n_{i\uparrow}(\tau)-n_{i\downarrow}(\tau)] \times[n_{i+l\uparrow}(0)-n_{i+l\downarrow}(0)]\rangle e^{iql}\,, \tag{2.4}$$

respectively, as a function of the temperature and the coupling constants. With an appropriate interchain Coulomb coupling (or electron transfer interaction leading to an effective spin exchange coupling) these susceptibilities can produce three-dimensional charge-density-wave (or spin-density-wave) phase transitions. It is also possible to have lattice instabilities associated with $N(q)$. Thus if the single-particle on-site energy [set equal to zero in Eq. (2.1)] were to vary under a lattice distortion,[15] a random-phase-approximation (RPA) treatment predicts a Peierls transition at a wave vector q and temperature T_c where

$$1=\frac{2|g_q|^2}{\omega_q}N(q)\,. \tag{2.5}$$

Here g_q is the electron-phonon coupling constant and ω_q is the phonon frequency. At temperatures just above T_c, the large amplitude vibration of the phonon associated with this soft-mode Kohn anomaly can give rise to a peak in the diffuse x-ray scattering.

We will also study the two-particle, two-hole susceptibility

$$N_V(q,0)=\int_0^\beta d\tau \sum_{i,l} \langle n_{i+1}(\tau)n_i(\tau) \times n_{i+l+1}(0)n_{i+l}(0)\rangle e^{iql} , \tag{2.6}$$

which enters in determining the instability of the lattice associated with a phonon modulation of the near-neighbor Coulomb interaction of the extended Hubbard model, Eq. (2.1). Alternatively, internal molecular vibrations can modulate the on-site Coulomb repulsion U.[16] In this case the relevant susceptibility is given by

$$N_U(q,0)=\int_0^\beta d\tau \sum_{i,l} \langle n_{i\uparrow}(\tau)n_{i\downarrow}(\tau) \times n_{i+l\uparrow}(0)n_{i+l\downarrow}(0)\rangle e^{iql} . \tag{2.7}$$

It is also interesting to determine various charge and spin structure factors corresponding to the equal-time correlation functions

$$S_\rho(q)=\frac{1}{N}\sum_{i,l}\langle (n_{i\uparrow}+n_{i\downarrow})(n_{i+l\uparrow}+n_{i+l\downarrow})\rangle e^{iql} \tag{2.8}$$

and

$$S_\sigma(q)=\frac{1}{N}\sum_{i,l}\langle (n_{i\uparrow}-n_{i\downarrow})(n_{i+l\uparrow}-n_{i+l\downarrow})\rangle e^{iql} . \tag{2.9}$$

In order to calculate these quantities we will use the Monte Carlo technique discussed in Refs. 5 and 6. The partition function for the system is written as

$$Z=\mathrm{Tr}e^{-\beta H}=\mathrm{Tr}\prod_{i=1}^{L} e^{-\Delta\tau H} , \tag{2.10}$$

with $\Delta\tau=\beta/L$. The Hamiltonian is decomposed into three parts as follows:

$$H_1=-t\sum_{i(\mathrm{even}),\sigma}(C_{i\sigma}^\dagger C_{i+1,\sigma}+\mathrm{H.c.}) ,$$

$$H_2=-t\sum_{i(\mathrm{odd}),\sigma}(C_{i\sigma}^\dagger C_{i+1,\sigma}+\mathrm{H.c}) , \tag{2.11}$$

$$H_{UV}=U\sum_i n_{i\uparrow}n_{i\downarrow}+V\sum_i n_i n_{i+1} ,$$

and the exponential is approximated by

$$\exp[-\Delta\tau(H_1+H_2+H_{UV})] =\exp\left[-\frac{\Delta\tau}{4}H_{UV}\right]e^{-\Delta\tau H_1}\exp\left[-\frac{\Delta\tau}{2}H_{UV}\right] \times e^{-\Delta\tau H_2}\exp\left[-\frac{\Delta\tau}{4}H_{UV}\right]+O((\Delta\tau)^2) . \tag{2.12}$$

Upon inserting complete sets of intermediate states between exponential factors, one obtains a representation of the one-dimensional quantum problem as a two-dimensional classical system on a "checkerboard" space-time lattice, as shown in Fig. 1 of Ref. 5. The degrees of freedom at each lattice point are the occupation number of spin-up and spin-down electrons. A repulsive interaction of strength $U/2$ acts between electrons of opposite spin at the same site, and a repulsion of strength $V/2$ between electrons at neighboring sites.

The time-slice size $\Delta\tau$ is determined by the accuracy desired. We have found that for the noninteracting problem, taking $\Delta\tau t=0.25$ gave reasonable accuracy (within a few percent) for most quantities of interest. The accuracy is best for the energy, and worst for correlation functions at points where divergences occur. For the interacting system, we have chosen $\Delta\tau\max(U,V)\lesssim 0.5$. Since the error in the decomposition (2.12) is proportional to the commutators of the different parts of the Hamiltonian, a smaller $\Delta\tau$ has to be taken when the interaction strength is increased. This limits somewhat the possibility of going to regimes of very large U and V, since increasingly more time slices have to be taken for a given temperature.

Throughout most of our study, we have taken a chain of twenty sites with periodic boundary conditions. By studying the effect of finite size in the noninteracting system, we concluded that finite-size effects are negligible for temperatures higher than $\beta t\sim 10$. Since the computation time increases only linearly with the size of the system, it is quite feasible to study lower temperatures by taking larger lattices in the space and time directions. Here, in units such that $t=1$, we have studied temperatures ranging from $\beta=3$ to $\beta=14.5$. For a bandwidth $4t=0.5$ eV, these correspond to temperatures ranging from approximately 500 to 100 K. There are small finite-size effects at the lowest temperature studied, $\beta=14.5$, on a 20-site lattice, but we estimated them to be within our statistical accuracy. The strength of the Coulomb interaction U is given in terms of t so that a U of 4 corresponds to a Coulomb coupling equal to the bandwidth. Results are given for $U=0$, 2, 4, 8, and ∞.

Figure 1 shows the charge-density susceptibility $N(q)$ at $\beta=7.25$ ($T\sim 200$ K for $4t=0.5$ eV) for the cases $U=0$ and $U=\infty$. Here, and throughout the paper, $N(q)$ and $\chi(q)$ will be measured in units of $2/\pi v_F$ with $v_F=\sqrt{2}$. This is just the low-temperature $q\to 0$ limit of $N(q)$ for a noninteracting one-quarter-filled chain. For $U=0$, $N(q)$ diverges logarithmically at $q=2p_F$, signaling the Peierls instability. At $U=\infty$, the Peierls instability occurs at $q=2\bar{p}_F$, with $\bar{p}_F$ the Fermi wave vector for the noninteracting spinless fermions, which is twice the original one. Thus in terms of the original p_F one obtains a logarithmic divergence at $q=4p_F$. The agreement between MC and exact results is reasonable in both limits, and converges for $\Delta\tau\ll 1$. For $\Delta\tau=0.25$ the Monte Carlo data overestimate the $U=0$ peak at $2p_F$ and underestimate the $U=\infty$ peak at $4p_F$ by about 10%. We expect similar accuracy in our numerical results for intermediate values of the coupling.

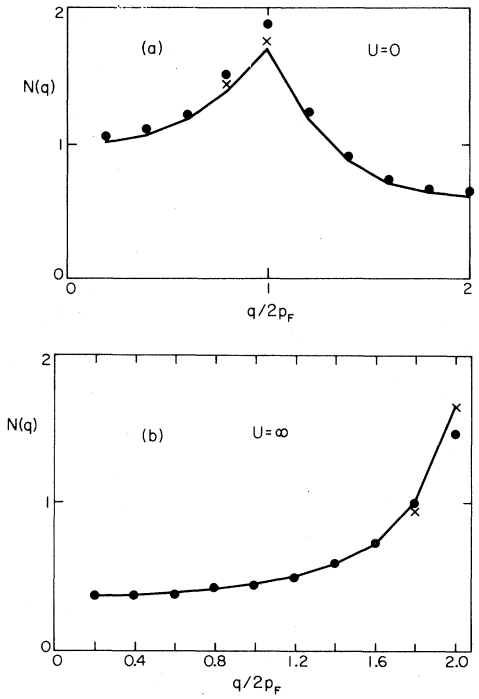

FIG. 1. (a) Zero-frequency charge-density susceptibility $N(q)$ normalized to $2/\pi v_F$ vs q for a 20-site system with $U=0$ and $\beta=7.25$. The solid line passes through the exact canonical result for a 20-site system with $U=0$ and $\beta=7.25$ and the points are Monte Carlo data with $\Delta\tau=0.25$. A similar Monte Carlo calculation with $\Delta\tau=0.125$ gives results which sit approximately midway between the points shown and the solid curve. Two of these are marked by $\times$'s. As $\Delta\tau$ goes to zero the Monte Carlo result converges to the exact canonical result. (b) $N(q)$ vs q with $U=\infty$ and $\beta=7.25$. As in Fig. 1(a), the solid line is the exact canonical result, the points are Monte Carlo data with $\Delta\tau=0.25$, and the $\times$'s are Monte Carlo data with $\Delta\tau=0.125$. Only two $\times$'s are shown because the others lay on the dots. Note that in the $U=\infty$ limit the peak occurs at $4p_F$.

For $U=0$, the spin-density correlation function is identical to the charge density. For large U and $V=0$, the model can be shown to be equivalent to an antiferromagnetic Heisenberg model as far as the spin degrees of freedom are concerned.[17] Therefore, the equal-time spin-density correlations are expected to decay as $1/R$ with distance.[18] Thus the spin-density structure factor will have a logarithmic divergence at $q=2p_F$, while the $\omega=0$ spin-density susceptibility will have a *linear* divergence at $q=2p_F$. For a finite system at finite temperatures, these divergences are cut off by the finite size or inverse temperature, whichever is smaller.

In Figs. 2(a) and 2(b) we show the charge-density structure function $S_\rho(q)$ for the cases $U=0$ and $U=\infty$, compared with exact results for the grand-

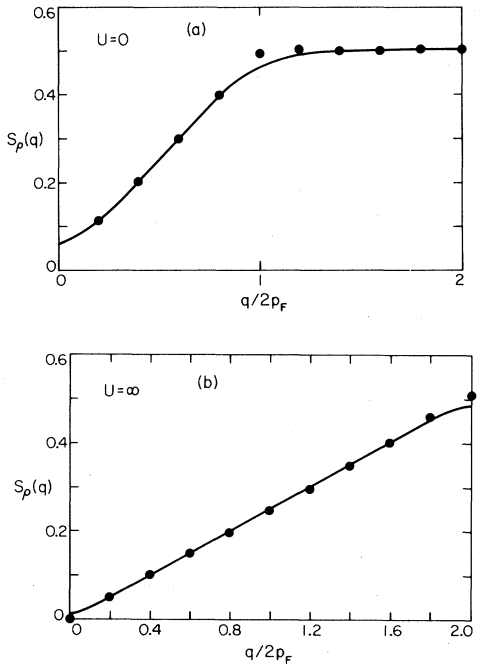

FIG. 2. (a) Charge-density structure factor $S_\rho(q)$ vs q for a noninteracting $U=0$, quarter-filled system with 20 sites at $\beta=7.25$. The solid line passes through the exact 20-site result for a grand-canonical ensemble at $\beta=7.25$ and the points are the Monte Carlo data for a canonical ensemble with $\Delta\tau=0.25$. (b) Charge-density structure factor $S_\rho(q)$ vs q for the quarter-filled $U=\infty$ limit. As in Fig. 2(a), the solid line represents the exact result for a grand-canonical ensemble while the points are Monte Carlo data appropriate to a canonical ensemble with $\Delta\tau=0.25$.

TABLE I. Singular behavior of the charge and spin structure factors and zero-frequency susceptibilities for an infinite chain in the limits $U=0$ and $U=\infty$.

	$S_\rho(q)$	$N(q)$	$S_\sigma(q)$	$\chi(q)$
$U=0$		$\ln T$ at $2p_F$		$\ln T$ at $2p_F$
$U=\infty$		$\ln T$ at $4p_F$	$\ln T$ at $2p_F$	$1/T$ at $2p_F$

canonical ensemble, at a temperature $\beta=7.25$. The case of the one-quarter-filled band at $U=\infty$ is exactly equivalent to a half-filled band of noninteracting *spinless* electrons as far as the charge degrees of freedom are concerned (except for certain small boundary effects). The agreement between the MC and exact results is very good except at some special points. Since our MC algorithm works in the *canonical* ensemble, it gives $S_\rho(q)=0$ for $q=0$. In the grand-canonical ensemble instead, $S_\rho(0)$ gives the fluctuation in particle number and is nonzero at finite temperatures. For the case $U=0$, the MC results give a sharper kink at $q=\pi/2$ than the grand-canonical results. The reason is that the smearing of the Fermi surface at finite temperature is larger in the grand-canonical than in the canonical ensemble. At $T=0$, the exact answer is a straight line up to $q=2p_F$ and a constant value for $q>2p_F$. Table I summarizes the singular behavior of the charge and spin structure factors and the static susceptibilities for an infinite chain in the limits $U=0$ and $U=\infty$.

We now discuss other properties of the system. Figure 3 shows the ground-state energy of the system as a function of U. The solid line is the exact result for the one-quarter-filled case calculated numerically by Shiba.[12] The curve starts from the $U=0$ result $E_0=-2\sqrt{2}/\pi$ and approaches the $U=\infty$ result of $E_0=-2/\pi$ for a half-filled band of noninteracting spinless fermions. The agreement with the Monte Carlo data obtained for $\beta=14.5$, our lowest temperature, is satisfactory.

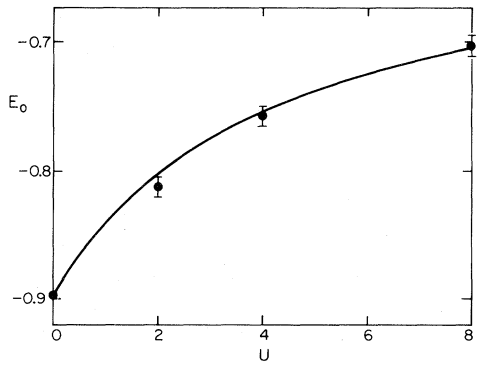

FIG. 3. Ground-state energy per site vs U for the quarter-filled sector. The solid curve is taken from Shiba's (Ref. 12) numerical solution, and the points are Monte Carlo data for a system of 20 sites at an inverse temperature $\beta=14.5$. All energies are measured in units of the hopping matrix element t.

Figure 4 shows MC results for the specific heat and susceptibility per site for the case $U=4, V=0$ as a function of temperature. The specific heat shows the two-peak structure found by Shiba and Pincus in their study of short chains.[19] The upper peak is associated with charge and the lower one with spin excitations of the system. The lower peak should occur at $T\sim J_{\rm eff}$ with $J_{\rm eff}$ the effective exchange interaction for the spins. We determined $J_{\rm eff}$ by assuming the relation for the zero-temperature susceptibility per spin of a Heisenberg chain,

$$\chi=\frac{g^2\mu_\beta^2}{2\pi^2 J_{\rm eff}}\ , \tag{2.13}$$

and using for χ the susceptibility per electron obtained by Shiba[12] from the exact solution. The result for the case under consideration is $J_{\rm eff}=0.14$, and is indicated by an arrow in Fig. 4. An alternative way of obtaining $J_{\rm eff}$ is from the strong coupling perturbation expansion of Klein and Seitz, which yields[17]

$$J_{\rm eff}=\frac{2t^2\rho}{U+(4t/\pi)\sin(\rho\pi)}\left[1-\frac{\sin(2\pi\rho)}{2\pi\rho}\right] \tag{2.14}$$

and gives $J_{\rm eff}=0.19$. The discrepancy with the previous result is due to the finite value of U.

Since our MC method works with a canonical en-

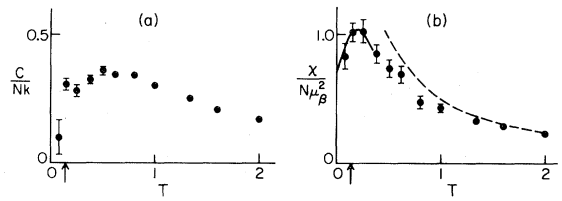

FIG. 4. Monte Carlo data for the specific heat and susceptibility per site of a system with $U=4$ and $V=0$. The arrow denotes a temperature where kT is equal to an effective exchange interaction $J_{\rm eff}$ given by Eq. (2.14). In (b), the solid curve is the Bonner-Fisher result for a Heisenberg chain and the dashed line is the Curie law for isolated spins.

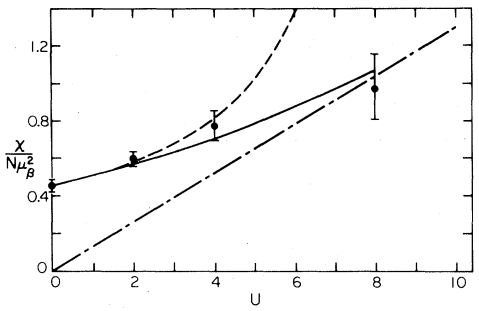

FIG. 5. Zero-temperature susceptibility per site vs U. The solid line was determined from Shiba's numerical results (Ref. 12). The short-dashed line is the enhanced Pauli susceptibility, Eq. (2.16), and the long-dash—short-dash line is the large U limit, Eq. (2.13). The Monte-Carlo data were obtained from $\chi(q)$ at the smallest nonzero q at the lowest temperature $\beta=14.5$.

semble, which has a fixed number of particles and fixed total spin, we cannot obtain the magnetic susceptibility directly. The MC results for $\chi(q=0)$ are always 0 because of the conservation of spin. However, the MC results for *finite* q should approach the correct results for the grand-canonical ensemble as $q\rightarrow 0$ with a q^2 dependence. We have simply taken the susceptibility to be the smallest nonzero q value

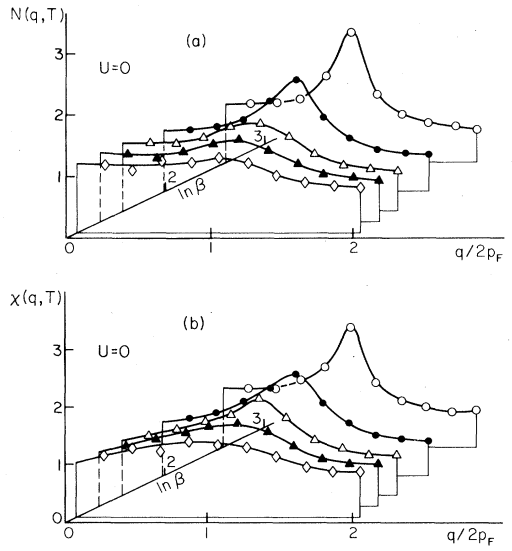

FIG. 6. Zero-frequency charge- and spin-density susceptibilities normalized to $2/\pi v_F$ vs q for $U=0$ and various temperatures. Here $\beta=t/kT$ and taking $4t=0.5$ eV the five profiles from front to back correspond to values of T approximately 500, 400, 300, 200, and 100 K, respectively. The solid lines are drawn through the Monte Carlo points as a guide to the eye. To within statistical errors, the results for (a) N and (b) χ are identical as they should be for $U=0$.

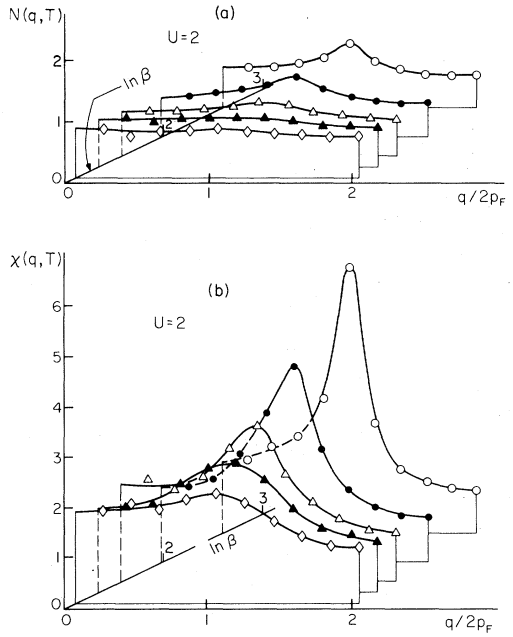

FIG. 7. Charge- and spin-density susceptibilities vs q for $U=2$ show the suppression of the peak at $2p_F$ in (a) N and the enhancement of the $2p_F$ peak in (b) χ produced by U in this temperature range.

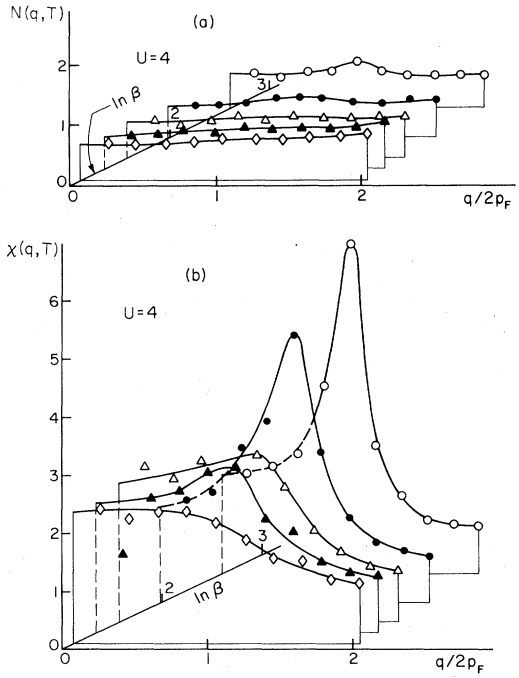

FIG. 8. (a) Charge- and (b) spin-density susceptibilities vs q for $U=4$. Note the nearly complete suppression of the $2p_F$ peak in N at the higher temperatures and the slight rise near $4p_F$ which goes away at lower temperatures as the peak near $2p_F$ returns.

of χ for our 20-site system, i.e.,

$$\chi(q=0)\sim\chi(q=2\pi/20)\ . \tag{2.15}$$

A somewhat more accurate procedure would be to fit the first points of $\chi(q)$ to a quadratic function to extract the $q=0$ value. However, we do not think that within our statistical accuracy that procedure would give different results. In Fig. 4(b), we indicate by a thin line the Bonner-Fisher[20] results for the Heisenberg model susceptibility, with $J_{\rm eff}$ given by Eq. (2.13). The MC results for the Hubbard model with $U=4$ appear to follow this behavior. The peak in the Bonner-Fisher susceptibility and in the MC results for the Hubbard model occurs at $T\approx 1.25J_{\rm eff}$. The dashed line in Fig. 4 represents the susceptibility per site of $N/2$ isolated spins, $\chi/N\mu_B^2=1/(2T)$. The MC results approach this behavior at high T, as expected. Although the statistical errors in Fig. 4 are rather substantial, it illustrates the fact that the MC procedures can be used to obtain thermodynamic properties. Better accuracy can be obtained by increasing the number of MC sweeps, but our primary interest here is in the study of $2p_F$ and $4p_F$ correlation functions.

Finally, we show in Fig. 5 the zero-temperature magnetic susceptibility as a function of U for the one-quarter-filled-band Hubbard model. The dashed line represents the weak coupling Pauli enhanced susceptibility[21]:

$$\frac{\chi}{N\mu_B^2}=\frac{2/\pi v_F}{1-U/2\pi v_F}\ . \tag{2.16}$$

For large U, the zero-temperature susceptibility for a one-quarter-filled band is given by Eq. (2.13) where to lowest order in t/U, $J_{\rm eff}=2t^2\rho/U$, which is t^2/U for $\rho=0.5$. This is indicated by a dash-dot line in Fig. 5. The exact result by Shiba interpolates smoothly between these limits and is shown as the solid line in Fig. 5. Our MC results for $U=0$, 2, 4, and 8 are shown as the solid dots.

III. RESULTS FOR THE CORRELATION FUNCTION

In this section we present numerical results for the Hubbard-model correlation functions. One question of particular interest is to see how the doubling of the characteristic wave vector for charge excitations occurs, from $2p_F$ at $U=0$ to $4p_F$ at $U=\infty$. One could imagine various possibilities: (1) The $2p_F$ peak for $U=0$ shifts its position continuously toward $4p_F$ as U is increased, (2) the disappearance of the $2p_F$ peak and the appearance of the $4p_F$ peak at a critical value of U, or (3) the coexistence of $2p_F$ and $4p_F$ singularities with relative strengths that depend on U. The spin-density singularity structure is somewhat simpler, since the divergence occurs at $q=2p_F$ for both $U=0$ and $U=\infty$ with different strengths, so that the most likely behavior is a singularity at $2p_F$ for arbitrary U with a strength that varies monotonically with U.

Figures 6–9 show the q dependence of the charge- and spin-density zero-frequency susceptibilities at various temperatures for the Hubbard model with $U=0$, 2, 4, and 8. We have chosen to compute these correlation functions at $\beta=3$, 3.75, 4.5, 7.25, and 14.5. As previously noted for $4t=0.5$ eV, these correspond approximately to temperatures of 500, 400, 300, 200, and 100 K, respectively. The value of $\Delta\tau$ was taken to be 0.25 for $U=0$ and $U=2$, 0.125 for $U=4$, and 0.0625 for $U=8$. For $U=0$ and $U=2$, 5000 measurements were made with 6 MC passes between measurements. As $\Delta\tau$ was decreased, the number of passes between measurements was increased proportionally, up to 24 for $U=8$. This is necessary because the acceptance fraction for the moves in our MC algorithm decreases as $\Delta\tau$ is decreased. Before starting the measurements, about 1000 warm-up sweeps were made to bring the system into equilibrium, with this number also increasing proportionally as $\Delta\tau$ was de-

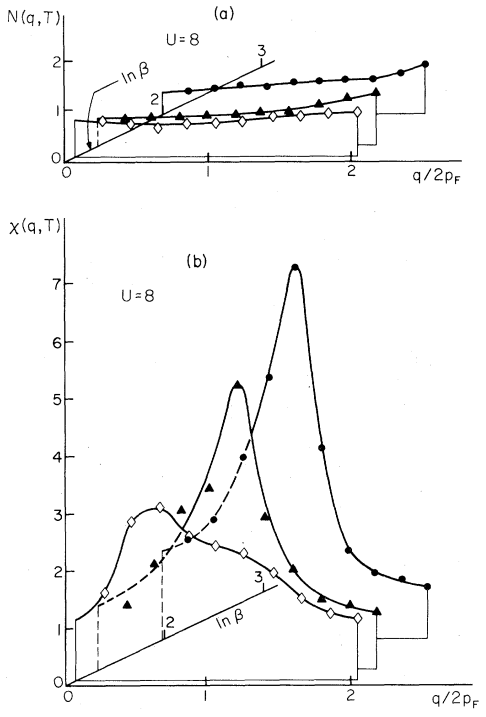

FIG. 9. Charge- and spin-density susceptibility vs q for $U=8$. Here $\beta=3$, 3.75, and 7.25, respectively. In N (a) there is no evidence of a $2p_F$ peak but there is a clear rise as q approaches $4p_F$. χ (b) shows a large $2p_F$ peak at low temperatures.

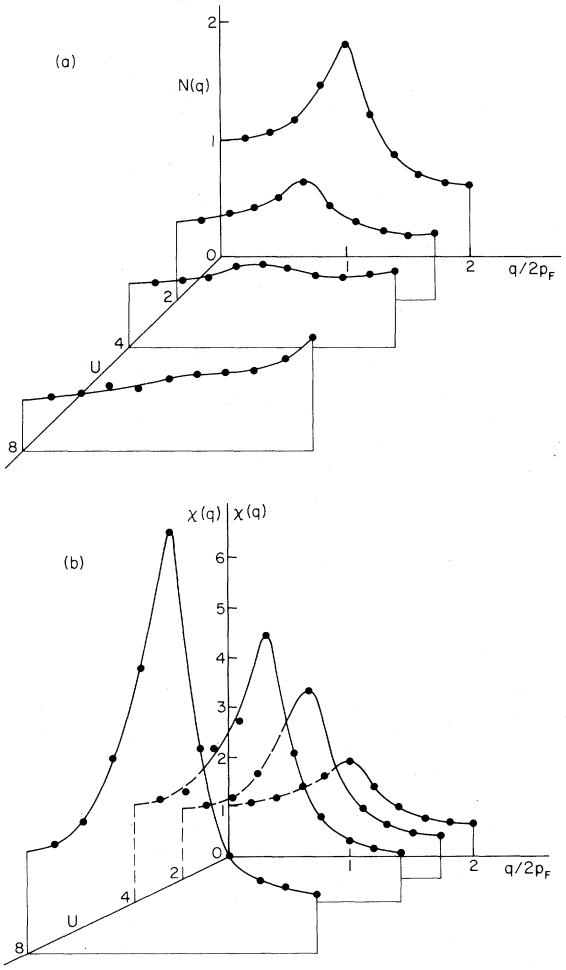

FIG. 10. (a) Charge- and (b) spin-density susceptibilities at $\beta=7.25$ for $U=0$, 2, 4, and 8. At fixed temperature, as U increases the peak in N at $2p_F$ decreases and a new peak appears at $4p_F$. The peak in χ at $2p_F$ is enhanced as U increases.

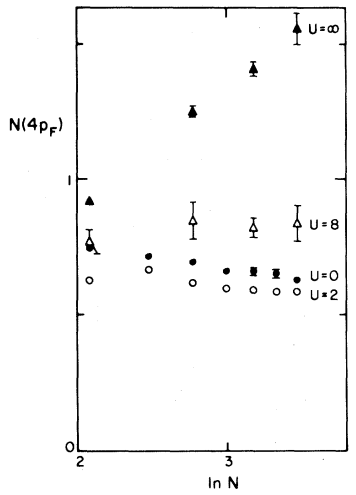

FIG. 11. $N(4p_F)$ vs $\ln N$ for various sized lattices with the number of τ slices $L=N$. With $\Delta\tau=0.25$ one has $\ln N=\ln(4t/kT)$ and one can view the figure as showing how $N(4p_F)$ scales with $\ln(4t/kT)$. For $U=\infty$ we see that $N(4p_F)\sim\ln(4t/kT)$ consistent with the expected $\ln(\epsilon_c/kT)$ behavior. For finite U these results indicate that $N(4p_F)$ does not diverge as $T\rightarrow 0$.

creased. For clarity, we do not show the statistical error in the MC data. In most cases, it was of order twice the size of the points. As U increased, it became somewhat larger for the spin-density correlation functions, and can be estimated approximately in the figures from the scatter of the MC data from a smooth line.

Figure 6 shows results for $U=0$. The solid lines here and in the following figures are drawn as smoothly as possible through the MC points to guide the eye. The results are identical for N and χ for this noninteracting case. Note the peak in these correlation functions at $q=2p_F$, which becomes sharper as the temperature is decreased. As mentioned earlier, the height of the peak diverges as $\ln(\epsilon_c/kT)$ for small T.

Figure 7 shows the susceptibilities for $U=2$. No $4p_F$ peak is yet noticeable in the charge-density susceptibility N. However, note the *weaker* $2p_F$ peak in N compared to the $U=0$ results. This is in contradiction to the fixed-point prediction of the RG, which has both N and χ diverging more strongly at $2p_F$ as U increases. We will return to this point in the next section. In contrast to the behavior of N, the $2p_F$ peak in χ has grown substantially in qualitative agreement with the fixed-point RG prediction.

In Fig. 8 we show results for $U=4$. At the highest temperature, N shows a small peak at $4p_F$. This peak increases slightly at the next lowest T, but then decreases and disappears as T is lowered. The $2p_F$ peak is almost nonexistent at the higher value of T, but appears as T is lowered. The spin-density response at $2p_F$ becomes now appreciably stronger, particularly at low temperatures.

Finally, we show in Fig. 9 results for $U=8$. Owing to the larger number of time slices and MC sweeps required for this case, we only show results for three temperatures: $\beta=3$, 3.75, and 7.25. The peak at $2p_F$ in N has now disappeared, and the $4p_F$ peak is somewhat larger, particularly at low temperatures. However, we cannot rule out the possibility that at even lower temperatures the $2p_F$ peak could reappear and the $4p_F$ peak disappear, as happened for $U=4$. The spin-density response at $2p_F$ is

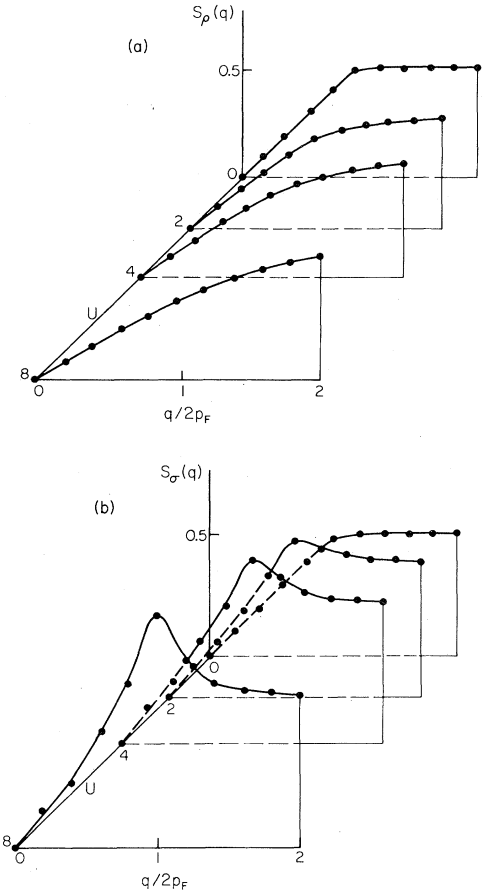

FIG. 12. (a) Charge-density and (b) spin-density structure factors $S_\rho(q)$ and $S_\sigma(q)$ vs q for various U values at $\beta=7.25$.

greatly enhanced, as expected.

In Fig. 10 we show the dependence of the charge- and spin-density susceptibilities on the interaction U for a fixed low temperature, $\beta=7.25$. As mentioned before, in N the $2p_F$ peak disappears, and the $4p_F$ peak develops as U is increased. For χ, the $2p_F$ peak becomes substantially stronger as U is increased.

We can draw some tentative conclusions from these results. For χ, the MC data indicate that the $2p_F$ response increases continuously as U is increased. The low-temperature behavior of the $2p_F$ peaks is most probably given by

$$\chi(2p_F) \propto \frac{1}{T^{\theta_\chi}} . \tag{3.1}$$

For $U=0$, the index $\theta_\chi=0$ corresponds to a logarithmic divergence, and for $U=\infty$, $\theta_\chi=1$ (see Table I). Within the weak coupling renormalization group one obtains $\theta_\chi=U/(2\sqrt{2}\pi t)$, which predicts that $\theta_\chi=1$ for $U/t=8.9$. It appears more likely, however, that the RG predictions break down before this and that θ_χ increases monotonically from 0 at $U=0$ to 1 at $U=\infty$. We will make a more detailed comparison with the RG predictions in the next section.

For the charge-density susceptibility, the results are somewhat less clear. We certainly do not see a simple peak that shifts its position from $2p_F$ to $4p_F$ as U is increased. The $2p_F$ peak persists but becomes smaller as U increases. However, as we will see in Sec. IV, there is reason to believe that at sufficiently low T it would increase beyond its $T\rightarrow 0$ value for small U. The $4p_F$ peak for small U appears to grow first but then decrease again as the temperature is further lowered [see particularly the $U=4$ results shown in Fig. 8(a)]. A simple picture that would explain this behavior is that there exists a crossover temperature $T_c(U)$ which goes to zero as $U\rightarrow\infty$. For $T>T_c$, the $4p_F$ peak *increases* as T is lowered, and for $T<T_c$, the $4p_F$ peak disappears. Conversely, the $2p_F$ peak only appears below the crossover temperature T_c. This picture implies that in the ground state there exists a $4p_F$ logarithmic singularity only at $U=\infty$, and that any finite U removes it. In terms of a global renormalization-group description, this behavior would correspond to the existence of an unstable fixed point for the charge degrees of freedom at $U=\infty$. The flow for any finite U would be toward the weak coupling regime, and the temperature T_c would measure the energy region over which the system behaves as if it were in the weak coupling regime. The dependence of T_c on U would be determined by the nature of the fixed points at $U=\infty$ and $U=0$.

In order to study the $4p_F$ behavior in more detail, we have looked at the $4p_F$ charge susceptibility for lattices of various sizes with $N=L$, up to $N=32$. Figure 11 shows the results plotted versus $\ln N$ for $U=0$, 2, 8, and ∞. For $U=\infty$, we see a straight line corresponding to a logarithmic divergence, as expected (see Table I). For finite U, the correlation function does not appear to diverge. Instead, it first increases and then levels off or even decreases, in accordance with the previous discussion. A more extensive Monte Carlo study using larger lattices would be needed to determine accurately the crossover temperature.

In Fig. 12 we show the charge- and spin-density structure factors $S_\rho(q)$ and $S_\sigma(q)$ for various U with $\beta=7.25$. The charge-density structure factor $S_\rho(q)$ evolves smoothly from the $U=0$ behavior (at $T=0$), a straight line from 0 to 0.5 for q from 0 to $2p_F$ and a constant value of 0.5 for $2p_F<p<4p_F$, toward the $U=\infty$ behavior which is a straight line from 0 at $q=0$ to 0.5 at $q=4p_F$. From Fig. 12(a) we see that no sharp peak appears at $4p_F$ for any value of U. The spin-density structure factor $S_\sigma(q)$

starts the same way as $S_\rho(q)$ for $U=0$, and develops a peak at $2p_F$ which diverges logarithmically at $U=\infty$. Presumably, for $U<\infty$ it takes a large but nondivergent value at $2p_F$ as $T\to 0$.

Finally, we discuss the behavior of the two-particle, two-hole correlation functions defined in Sec. II, Eqs. (2.6) and (2.7). Figure 13 shows $N_U(q)$ for $\beta=7.25$ at three values of U ($U=0$, 8, and ∞). Note that $N_U(q)$ shows a peak at $2p_F$ for $U=0$. This is because a piece of this correlation function corresponds to the particle-hole susceptibility. For $U=0$, we can write

$$N_U(q)=N_U^I(q)+\tfrac{1}{16}N(q)\ , \tag{3.2}$$

and the two-particle, two-hole irreducible part $N_U^I(q)$ shows no divergence at all. As U is increased, this correlation function is rapidly suppressed because the number of doubly occupied sites is reduced.

Figure 14 shows the function $N_V(q)$ for $\beta=7.25$ and $U=0$, 8, and ∞. Again we can write a decomposition such as Eq. (3.2) both for $U=0$ and $U=\infty$ in which the irreducible two-particle, two-hole part $N_V^I(q)$ is separated from the single-particle–hole part. The irreducible part $N_V^I(q)$ can be shown to be a smooth function with no singularities both at $U=0$ and $U=\infty$. In these limits the singularities in $N_V(q)$ come entirely from the single-particle–hole channel. In Fig. 15 we reproduce the single-particle–hole charge-density susceptibility $N(q)$ for the same parameters as those used in Fig. 14 for $N_V(q)$. The peak that appears in Fig. 14 for $q\to 4p_F$ at $U=\infty$ is solely due to the $q\to 4p_F$ behavior of the single-particle–hole piece (see Fig. 15). A coherence factor arising from the near-neighbor $n_{l+1}n_l$ form of the operators appearing in $N_V(q)$ suppresses the $U=0$ structure in $N_V(q)$ at $q=2p_F$ which is seen in $N(q)$.

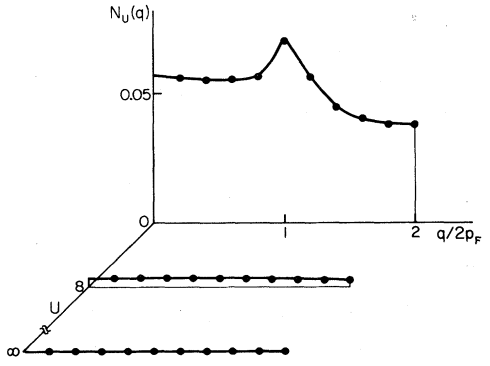

FIG. 13. Two-particle, two-hole susceptibility $N_U(q)$ at $\beta=7.25$ vs q for $U=0$, 8, and ∞. The peak at $2p_F$ in the $U=0$ response arises from the single-particle–hole part of $N_U(q)$.

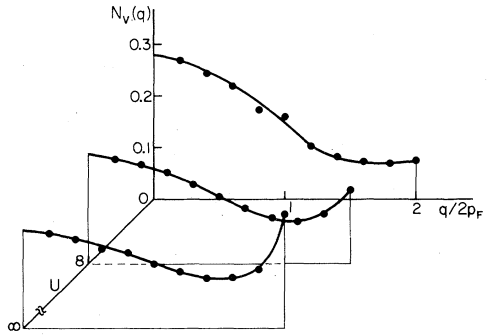

FIG. 14. Two-particle, two-hole susceptibility $N_V(q)$ at $\beta=7.25$ vs q for $U=0$, 8, and ∞.

For intermediate values of U we cannot make a separation such as Eq. (3.2); however, we can study the behavior of the $4p_F$ peak in $N_V(q)$ versus lattice size. Figure 16 shows how $N_V(q)$ scales with $\ln N$ for $U=0$, 2, 8, and ∞. Note how similar these results are to those of the charge susceptibility shown in Fig. 11 and that a divergence seems to occur only at $U=\infty$. Thus for finite U we find no evidence for a singular $4p_F$ response in the two-particle, two-hole channel generated by on-site or near-neighbor operators in the Hubbard model. Emery has pointed out that for the one-quarter-filled band one would not expect a singular $4p_F$ response in N_V due to coherence factors in $\sum_l n_{l+1}n_l e^{iql}$ but that the susceptibility associated with the next-nearest-neighbor operator $\sum_l n_{l+2}n_l e^{iql}$ may be singular.[22]

IV. COMPARISON OF MONTE CARLO DATA WITH RENORMALIZATION-GROUP RESULTS

As one knows, the zero-frequency, $2p_F$ charge-density and spin-density susceptibilities for a noninteracting one-dimensional electron gas have a low-temperature logarithmic divergence

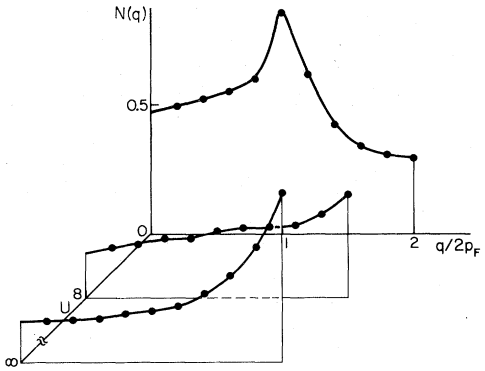

FIG. 15. Single-particle–hole charge-density susceptibility $N(q)$ at $\beta=7.25$ vs q for $U=0$, 8, and ∞. Here we have not divided $N(q)$ by $2/\pi v_F$.

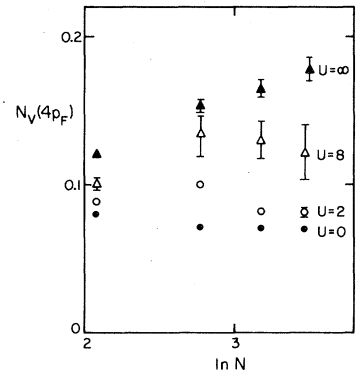

FIG. 16. $N_V(4p_F)$ vs $\ln N$ for various sized lattices with $N=L$. For $U=\infty$, $N_V(4p_F)\sim\ln N$ implying a $\ln(\epsilon_c/kT)$ divergence due to the contribution of the single-particle–hole channel. At finite values of U, $N_V(4p_F)$ does not diverge. Compare with Fig. 11.

$$N(2p_F)=\chi(2p_F)=\tfrac{1}{2}\ln(\epsilon_c/kT)\ . \tag{4.1}$$

Here we have followed our convention of normalizing these with respect to $2/\pi v_F$. Applying perturbation theory to the Hubbard model, Eq. (2.1) with $V=0$, generates a sequence of logarithmic corrections involving successive powers of $(U/\pi v_F)\ln(\epsilon_c/kT)$. Clearly, even when $U/\pi v_F$ is small, perturbation theory will fail at a sufficiently low temperature.

To deal with these diverging logarithms, Menyhard and Solyom[3] applied a renormalization-group approach. Here attention is focused on states near the Fermi surface $\pm p_F$, and the electron dispersion relation is approximated by the linear form $\epsilon_p=v_F(\,|p|-p_F)$ with a bandwidth cutoff $\pm\epsilon_c$. The interaction is parametrized in terms of a coupling constant g_2 which characterizes small momentum transfers, and g_1 which characterizes large momentum transfers of order $2p_F$ in which electrons are scattered across the Fermi surface. The basic idea of the renormalization group is to map the original problem with a cutoff energy ϵ_c and coupling constants g_1 and g_2 onto another equivalent problem in which the cutoff has been reduced and the couplings correspondingly altered. Reducing the cutoff implies eliminating degrees of freedom. When the cutoff is reduced to order kT, the logarithmic terms are no longer dangerous and, at least for weak coupling, perturbation theory can be used. Since the cutoff energy ϵ_c enters in terms of the parameter $l=\ln(\epsilon_c/kT)$ we will find it physically more useful to view ϵ_c as fixed and kT as changing. At larger values of kT where $l\simeq 0$ we will use perturbation theory to solve the original problem and then scale to low temperatures where l is large using the renormalized l-dependent couplings.

To implement these ideas, Menyhard and Solyom used a multiplicative renormalization transformation calculated in perturbation theory. In second order they found that the effective l-dependent coupling constants are given by

$$\frac{dg_1(l)}{dl}=-[g_1^2(l)+\tfrac{1}{2}g_1^3(l)]\ ,$$
$$g_2(l)=g_2(0)-\frac{g_1(0)}{2}+\frac{g_1(l)}{2}\ . \tag{4.2}$$

Here $g_2(0)$ and $g_1(0)$ are the unrenormalized coupling constants of the original problem which for the Hubbard model are both equal to $U/\pi v_F$. For the repulsive Hubbard model ($U>0$), as the temperature is lowered and l goes from 0 toward ∞, the effective couplings flow toward smaller values ending at the fixed point $g_2^*=U/2\pi v_F$ and $g_1^*=0$. If $U/\pi v_F$ is small to start with, perturbation theory can be used over the entire range to construct the RG.

Thus in the low-temperature limit, the large momentum (backward scattering) coupling vanishes leaving a Tomonoga-Luttinger model whose solution is known.[2,3] In particular, the zero-frequency charge and spin susceptibilities at $2p_F$ both diverge, neglecting logarithmic correction, as

$$(\epsilon_c/kT)^{\alpha}\ , \tag{4.3}$$

with

$$\alpha=1-\frac{(1-g_2^*)^{1/2}}{(1+g_2^*)^{1/2}}\cong g_2^*+O(g_2^{*2})\ . \tag{4.4}$$

Based upon this fixed-point behavior, the ground-state phase is said to be characterized as having both

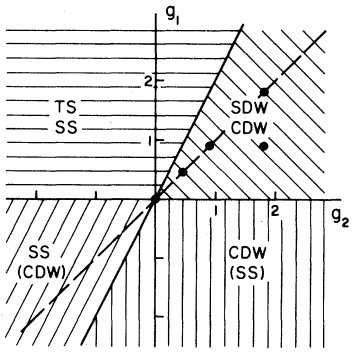

FIG. 17. Phase diagram of a one-dimensional electron gas obtained from the second-order renormalization-group approximation. Coupling constants for the Hubbard model lie along the dashed line $g_1=g_2$. The dots show the cases that have been studied numerically in this paper.

a divergent CDW and SDW response.

As discussed in Sec. II, the low-temperature phase of a quasi-one-dimensional system depends on both the strength of the single-chain susceptibility and the interchain coupling. Within the RG approach, the fixed-point power-law exponent which determines the ground-state response has been used to characterize the strength of the single-chain susceptibilities. With the use of this criterion, one obtains the well-known phase diagram for the one-dimensional (1D) Fermi gas shown in Fig. 17. Here SS and TS stand for singlet and triplet superconductivity, respectively. The labels denote regions in which the correspondingly susceptibilities exhibit power-law divergencies. Parentheses enclose responses which have a lower power-law degree of divergence than that of the dominant response in their region.

In Fig. 17 the Hubbard model corresponds to the dashed line where $g_1=g_2=U/\pi v_F$. The dots along this line correspond to values of $U=0$, 2, 4, and 8. For the extended Hubbard model

$$g_1=[U+2V\cos(2p_F)]/\pi v_F\ ,$$
$$g_2=(U+2V)/\pi v_F\ , \tag{4.5}$$

with $v_F=2t\sin p_F$. For the one-quarter-filled case which we are studying $p_F=\pi/4$, so that $g_1=U/\pi v_F$ and $g_2=(U+2V)/\pi v_F$. The remaining dot in Fig. 17 corresponds to the extended Hubbard model with $U=4, V=2$ which is discussed in Sec. V.

From our Monte Carlo results it is apparent that the zero-frequency, $2p_F$ spin-density susceptibility is enhanced by U while the corresponding charge-density susceptibility is suppressed in disagreement with the fixed-point behavior just discussed. In order to understand this it is useful to examine the first-order perturbation-theory corrections to the noninteracting susceptibilities,

$$N(2p_F)=\frac{1}{\pi v_F}\ln\left[\frac{\epsilon_c}{kT}\right]\left[1-\frac{2g_1-g_2}{2}\ln\left[\frac{\epsilon_c}{kT}\right]\right],$$
$$\chi(2p_F)=\frac{1}{\pi v_F}\ln\left[\frac{\epsilon_c}{kT}\right]\left[1+\frac{g_2}{2}\ln\left[\frac{\epsilon_c}{kT}\right]\right]. \tag{4.6}$$

Setting $g_1=g_2=U/\pi v_F$ it is clear that to this order in perturbation theory, $N(2p_F)$ is suppressed and $\chi(2p_F)$ is enhanced by the interaction.

By differentiating these expressions with respect to $l=\ln(\epsilon_c/kT)$, reduced susceptibilities which scale can be constructed. Using the second-order results of Menyhard and Solyom,[3] one finds

$$N(2p_F,l)=C_1\int_0^l dl_1\exp\left[\int_0^{l_1}dl_2[g_2(l_2)-2g_1(l_2)-F(l_2)]\right]+C_2$$

and

$$\chi(2p_F,l)=C_1'\int_0^l dl_1\exp\left[\int_0^{l_1}dl_2[g_2(l_2)-F(l_2)]\right]+C_2'\ , \tag{4.7}$$

with

$$F(l)=\tfrac{1}{2}[g_1^2(l)-g_1(l)g_2(l)+g_2^2(l)]\ . \tag{4.8}$$

In order to proceed, the constants C_1, C_2 and an effective cutoff ϵ_c must be specified. For the noninteracting system it is also possible to absorb C_2 into an effective value for ϵ_c. Monte Carlo data taken as described below, for the noninteracting system, fits

$$N(2p_F)=\frac{1}{\pi v_F}\ln\left[\frac{4t}{kT}\right]. \tag{4.9}$$

The coefficient $1/\pi v_F$ is just what one would calculate. A simple choice of constants for Eq. (4.7) which gives Eq. (4.9) is $C_1=1/\pi v_F$, $C_2=0$, and $\epsilon_c=4t$. We will use these values along with similar values for C_1', and C_2' in our subsequent discussion.[23]

Note that according to Eqs. (4.7) and (4.8), at high temperature both N and χ vary as $\ln(\epsilon_c/kT)$ in agreement with Eq. (4.1). At low temperatures, where l is large, both N and χ diverge as

$$\exp[l(g_2^*-\tfrac{1}{2}g_2^{*2})]=\left[\frac{\epsilon_c}{kT}\right]^{(g_2^*-\frac{1}{2}g_2^{*2})}. \tag{4.10}$$

Here $g_2^*=U/2\pi v_F$ is the leading contribution to the index α and $-\frac{1}{2}g_2^{*2}$ is just the next term out in the expansion of the square-root solution of the Tomonaga-Luttinger model, Eq. (4.4).

It is straightforward to integrate the nonlinear renormalization-group equations (4.2) to obtain $g_1(l)$ and $g_2(l)$. Using these in Eq. (4.7), we find the behavior shown in Fig. 18. The long-dash, short-dash line shows the $\ln(\epsilon_c/kT)$ divergence of the noninteracting $2p_F$ susceptibilities as the temperature is lowered. The solid lines give the behavior for the $2p_F$ spin susceptibility for two values of U and similarly the dashed lines show the charge-density response. Initially, for small l, as the temperature is lowered the effect of the Coulomb interaction is to enhance χ and to suppress N. Finally, at ultra low temperature where $l>10$, the charge-density

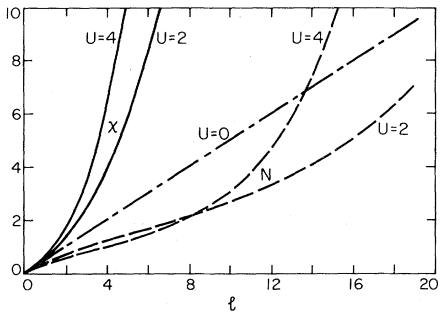

FIG. 18. Renormalization-group results for the $2p_F$ susceptibilities vs $l=\ln(\epsilon_c/kT)$ for different values of U. The long-dash—short-dash line is the noninteracting $U=0$ result. The solid lines are the spin susceptibility for $U=4$ and 2 and the dashed curves are the charge-density susceptibility for $U=4$ and 2.

response N rises and eventually diverges with the same power law as χ.[24] As previously discussed we are interested in systems in which ϵ_c is a few tenths of an electron volt and low temperatures are of order 100 K. This implies l values less than 4. An l value of 10 would correspond to a temperature less than one degree well below the typical Peierl's transition temperature for materials such as TFF-TCNQ. Hence the fixed-point solution is not relevant.

It is interesting to test our Monte Carlo results against the renormalization-group results. We have done this by calculating $N(2p_F)$ and $\chi(2p_F)$ on different sized lattices. Fixing $\Delta\tau$ at 0.25 we varied the number of time slices to obtain different values of ϵ_c/kT. In these calculations the number of lattice sites N was set equal to the number of time slices so that $t/kT=0.25N$ and

$$l=\ln(\epsilon_c/kT)=\ln N\ . \tag{4.11}$$

We have plotted in Fig. 19 the Monte Carlo results for $N(2p_F)$ and $\chi(2p_F)$ vs l for different values of the Coulomb interaction U. This corresponds to a

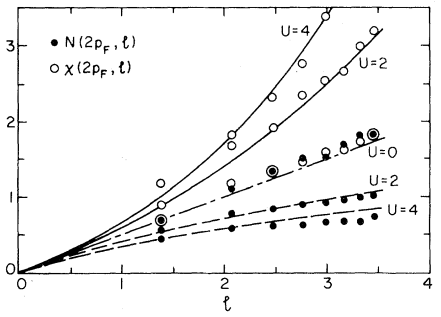

FIG. 19. Blowup of the region around the origin of Fig. 18 comparing Monte Carlo data with the predictions of the second-order renormalization-group equations.

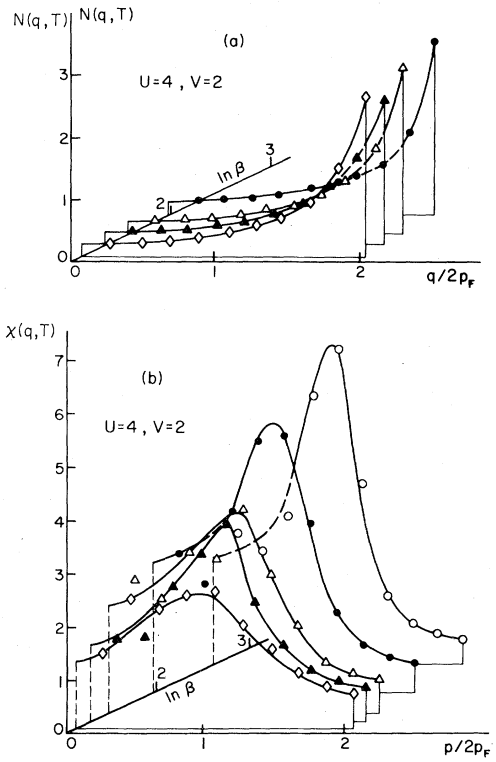

FIG. 20. (a) Charge- and (b) spin-density susceptibilities vs q for $U=4, V=2$ and various temperatures. Note the sharp peak at $4p_F$ in the charge density, as well as the complete suppression of the $2p_F$ peak. Note also the much weaker temperature dependence of the charge-density $4p_F$ susceptibility as compared to the $2p_F$ peak in the spin-density response.

blowup of the origin of Fig. 18. The long-dash line is again the noninteracting result while the solid lines and dashed lines correspond to N and χ, respectively, for $U=2$ and 4. The Monte Carlo results for the charge density are shown as solid points and the spin density as open points. Runs were carried out for $U=0$, 2, and 4.

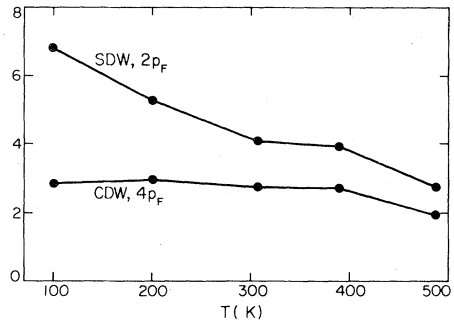

FIG. 21. Temperature dependence of the $4p_F$ charge- and spin-density susceptibility peaks for the case $U=4, V=2$. The temperature scale corresponds to the case $4t=0.5$ eV.

V. EXTENDED HUBBARD MODEL

We have seen in Sec. III that a Hubbard model with only on-site interactions does not give an appreciable $4p_F$ response for reasonable values of U; indeed it appears that the response only becomes singular at $U=\infty$. In principle, the long-range Coulomb interaction between electrons can give rise to interactions U, V, V_2, V_3, . . . , for electrons located on the same molecule, nearest-neighbor molecules, etc. Here we consider the effect of adding the nearest-neighbor repulsion term V to the Hubbard Hamiltonian. For the case considered here, the one-quarter-filled band, it can easily be seen that V can have a dramatic effect on the $4p_F$ response. Consider the limiting case $U=\infty$. Then, the system becomes equivalent to a half-filled band of spinless fermions with a nearest-neighbor repulsion V. It is well known that this system undergoes a transition to a CDW state at $V=2t$.[5] In the present context, we would describe the system for $V>2t$ as a Wigner crystal, since there is long-range order in the charge degrees of freedom, with period $4p_F$.

We have looked at the particular case $U=4, V=2$. The charge-density susceptibility is shown in Fig. 20(a). Note the sharp rise at $q=4p_F$, in contrast to the case $U=4, V=0$ [Fig. 8(a)]. It can be seen that there is only a weak dependence of the charge-density susceptibility on temperature. Note also that the $2p_F$ peak has now completely disappeared, and the function rises monotonically from 0 to $4p_F$. The spin-density response is shown in Fig. 20(b). There is an enhancement in this correlation function when V is turned on [compared with Fig. 8(b)]. In Fig. 21 we have plotted the amplitude of the $4p_F$ peak in N and the $2p_F$ peak in χ as a function of temperature. Note that the $4p_F$ peak shows little temperature dependence while the $2p_F$ peak in χ increases as the temperature is lowered. Torrance[10] has argued that the temperature dependence of the charge-density response should be small because the Coulomb interactions are large compared to kT, while the spin-density response should be temperature dependent because the effective magnetic exchange coupling between the spins is expected to be a few hundred degrees. (For the case $U=4, V=0$, we obtained in Sec. II, $J_{\text{eff}} \cong 200$ K.)

In Fig. 22 we show the charge and spin structure factors $S_\rho(q)$ and $S_\sigma(q)$ for $U=4$ and $V=2$ at $\beta=7.25$. In the spin structure factor, we see some enhancement with respect to the $U=4, V=0$ case, as expected. The charge structure factor rises gradually as $q \to 4p_F$ but no sharp peak is observed.

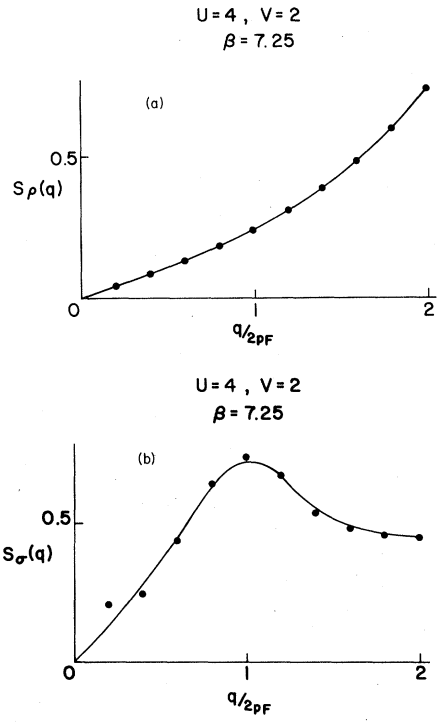

FIG. 22. (a) Charge- and (b) spin-density structure factors vs q for $U=4, V=2$ at $\beta=7.25$.

VI. CONCLUSIONS

As shown by these examples, Monte Carlo simulation can provide detailed information on the properties of a one-dimensional electron system. It allows us to directly calculate a variety of observable quantities. Furthermore, one can compare the results of the simulations for various limiting cases with exact results giving one a measure of confidence in the procedure which is then straightforward to extend to intermediate regions of parameter space where one does not have exact results. Also, as shown, the nature of the singular structure at low temperatures for an infinite system can be explored using finite-size scaling techniques.

Naturally, there are a variety of further questions suggested by this study. An important problem, currently under investigation, is the effect of different charge fillings on the properties of the Hubbard model. We have previously reported some results for the half-filled-band case ($\rho=1.0$). We are presently running simulations for intermediate ρ values between 0.5 and 1.0. In addition, other response functions are of interest. For example, the transfer-charge-density susceptibility

$$\tilde{N}(q)=\int_0^\beta d\tau \sum_{l\sigma\sigma'} \langle C^\dagger_{i+l\sigma}(\tau) C_{i+l+1\sigma}(\tau) \times C_{i+l\sigma'}(0) C_{i\sigma'}(0) \rangle e^{iql} \tag{6.1}$$

determines the response of the electrons to a variation in the electron-transfer term t. Just as $N(q)$ determines the stability of the lattice with respect to deformations which alter the on-site single-particle energy, $\tilde{N}(q)$ determines the stability of the lattice with respect to modulations of t. Thus the full exploration of this system forms a wide area for further research. Here we conclude by summarizing the results which we have so far obtained for the *one-quarter-filled-band* Hubbard model.

(1) Coulomb interactions suppress the $2p_F$ peak in the charge-density susceptibility over the range of physically relevant temperatures. For the Hubbard model with only an on-site U, the $T\rightarrow 0$ limit may diverge as predicted by the RG equations, but this divergence occurs at unphysically low temperatures and over the temperature range of interest the $2p_F$ charge-density susceptibility is substantially weaker at finite U than for $U=0$. In the presence of a moderate nearest-neighbor interaction V, the $2p_F$ peak is completely suppressed. Thus contrary to the well-known fixed-point RG result,[25] the effect of Coulomb interactions is to suppress the charge-density-driven Peierls instability.

(2) The $2p_F$ spin-density susceptibility is greatly enhanced by a finite U, and even more in the presence of a finite V.

(3) The $4p_F$ charge-density susceptibility in the one-dimensional Hubbard model with only an on-site interaction is very weak. Most probably, it is only logarithmically divergent at $U=\infty$, and nonsingular for $U<\infty$. In the presence of a moderate nearest-neighbor interaction V, the $4p_F$ charge-density peak is greatly enhanced. It is interesting to note that we do not find a (U,V) parameter range for which there is a coexistence of $2p_F$ and $4p_F$ charge-density instabilities.[26]

(4) The irreducible two-particle, two-hole correlation functions of the Hubbard model generated by $n_{i\uparrow}n_{i\downarrow}$ and $n_{i+1}n_i$ are not divergent at $U=0$ and $U=\infty$. At intermediate values of U we cannot separate the single-particle—hole charge-density part of the response, but our scaling analysis showed that the behavior of the $4p_F$ peak in these two-particle, two-hole susceptibilities is similar to the behavior of the $4p_F$ peak in the charge-density response. In particular, for finite U, the peak at $4p_F$ is nonsingular as $T\rightarrow 0$.

Note added in proof. Preliminary results for $\tilde{N}(q)$, Eq. (6.1), do show coexistance of $2p_F$ and $4p_F$ instabilities for a certain range of (U,V) parameters.

ACKNOWLEDGMENTS

We are grateful to R. L. Sugar for providing us with the exact canonical results used in Fig. 1, as well as for many useful discussions. We are also grateful to V. Emery, P. Pincus, J. B. Torrance, W. Kohn, and J. R. Schrieffer for simulating discussions. This work was supported by the National Science Foundation under Grants Nos. PHY-77-27084 and DMR-80-01492. We would also like to acknowledge support from the University of California Regents' Fund.

[1]See, for example, *Recent Developments in Condensed Matter Physics,* edited by J. T. Devreese (Plenum, New York, 1981), Vol. 1, Chap. 8, and references therein.

[2]V. J. Emery, in *Highly Conducting One-Dimensional Solids,* edited by J. Devreese, R. Evrard, and V. Van Doren (Plenum, New York, 1979), p. 247.

[3]N. Menyhard and J. Solyom, J. Low Temp. Phys. 12, 529 (1973); J. Solyom, Adv. Phys. 28, 201 (1979).

[4]J. Hubbard, Proc. R. Soc. London Ser. A 276, 238 (1963).

[5]J. E. Hirsch, D. J. Scalapino, R. L. Sugar, and R. Blankenbecler, Phys. Rev. Lett. 47, 1628 (1981).

[6]J. E. Hirsch, R. L. Sugar, D. J. Scalapino, and R. Blankenbecler, Phys. Rev. B 26, 5033 (1982).

[7]J. E. Hirsch and E. Fradkin, Phys. Rev. Lett. 49, 402 (1982).

[8]R. E. Peierls, *Quantum Theory of Solids* (Oxford University Press, London, 1955), p. 108.

[9]R. Comes and G. Shirane, *Highly Conducting One-Dimensional Solids,* edited by J. T. Devreese, R. P. Evrard, and V. E. Van Doren (Plenum, New York, 1979), p. 17; S. Kagoshima, in *Extended Linear Chain Compounds,* edited by J. S. Miller (Plenum, New York, 1982), Vol. 2, p. 303.

[10]J. B. Torrance, Phys. Rev. B 17, 3099 (1978); also see J. Bernasconi, M. J. Rice, W. R. Schneider, and S. Strässler, Phys. Rev. B 12, 1090 (1975).

[11]V. J. Emery, Phys. Rev. Lett. 37, 107 (1976).

[12]H. Shiba, Phys. Rev. B 6, 930 (1972).

[13]H. Gutfreund and R. A. Klemm, Phys. Rev. B 14, 1073 (1976); 14, 1086 (1976).

[14]L. H. Lieb and F. Y. Wu, Phys. Rev. Lett. 20, 1445 (1968).

[15]For example, in TTF-TCNQ the π electrons may have an appreciable coupling to the intramolecular vibrational modes. M. J. Rice and N. O. Lipori, Phys. Rev. Lett. 38, 437 (1977).

[16]P. Pincus, Solid State Commun. 11, 51 (1972).

[17]D. J. Klein and W. A. Seitz, Phys. Rev. B 10, 3217 (1974).

[18]A. Luther and I. Peschel, Phys. Rev. B 12, 3908 (1975).

[19]H. Shiba and P. Pincus, Phys. Rev. B 5, 1966 (1972).

[20]J. C. Bonner and M. E. Fisher, Phys. Rev. 135, A640 (1964).

[21]I. E. Dzyaloshinsky and A. I. Larkin, Zh. Eksp. Teor. Fiz. 61, 791 (1971) [Sov. Phys—JETP 38, 202 (1971)]; H. Fukuyama, T. M. Rice, C. M. Varma, and B. I. Halperin, Phys. Rev. B 5, 3775 (1974).

[22]V. Emery (private communication).

[23]Rather than lump C_2 into ϵ_c one might have taken $\epsilon_c \cong t$ and adjusted C_2 to fit the high-temperature (small lattice) end of the MC data for each U. It turns out that this does not give a very good fit to our data. It appears we need $\epsilon_c \cong 4t$ rather than t. In the RG, the various logarithmically singular terms are of course accompanied by constant terms which, if put into the $\ln(\epsilon_c/kT)$ term can alter the value of ϵ_c.

[24]A qualitatively similar behavior was observed by P. A. Lee, T. M. Rice, and R. A. Klemm, Phys. Rev. B 15, 2984 (1977) in a study of the role of interchain coupling. In this work the crossover temperature at which N begins to diverge is much larger than we find. This is due to both the effects of interchain coupling and the fact that only the lowest-order terms were kept. We see a shift of the crossover temperature to a high temperature if F is neglected in Eq. (4.7).

[25]S. T. Chui, T. M. Rice, and C. M. Varma, Solid State Commun. 15, 155 (1974).

[26]This is in disagreement with results from computer renormalization-group calculations of $N(q)$ reported by S. T. Chui and J. W. Bray, Phys. Rev. B 21, 1380 (1980).